RSC Advances

PAPER

View Article Online
View Journal | View Issue

Open Access Article. Published on 20 September 2021. Downloaded on 11/9/2025 1:16:10 AM.
This article is licensed under a Creative Commons Attribution-NonCommercial 3.0 Unported Licence.

Check for updates

Cite this: *RSC Adv.*, 2021, **11**, 30990

Isolation of HLA-G$^+$ cells using MEM-G/9 antibody-conjugated magnetic nanoparticles for prenatal screening: a reliable, fast and efficient method

Elaheh Emadi,[a] Abdol-Khalegh Bordbar,[†bc] Hamid Nadri,[d] Ali Shams,[e] Asghar Taheri-Kafrani[f] and Seyed Mehdi Kalantar[†*ag]

Received 7th August 2021
Accepted 13th September 2021

DOI: 10.1039/d1ra05988b

rsc.li/rsc-advances

The development of an effective and noninvasive early method for obtaining fetal cells is crucial to prenatal screening. Despite proving the presence of fetal cells in the reproductive tract, their use is limited due to their inability to properly isolate them from maternal cells. Magnetic-activated cell sorting (MACS) is a simple technique to separate cells. The present study aimed to develop a MACS-based platform for the isolation of the HLA-G expressing trophoblast cells. For this purpose, first, the triazine functionalized MNPs were synthesized and characterized. Then, MNPs were directly and indirectly conjugated by the MEM-G/9 antibodies targeting HLA-G$^+$ cells. The antibody amount on the surface of the nanoparticles was determined with the Bradford assay. The cell capture efficiency was also investigated. Various characterization methods confirmed the successful nanoparticle synthesis and antibody conjugation. The optimal initial antibody amount for the immobilization was about 20 μg and the optimal time was 3 h. The antibody-nanoparticles by the indirect method had better targeting and capture efficiency than the direct method. The MNPs indirectly conjugated with antibodies are an efficient tool for cell isolation and present considerable potential to be applied in biomedical fields.

1 Introduction

The advanced reproductive age increases the risk of having a newborn with a structural or a chromosomal abnormality.[1] A prenatal diagnostic procedure that can provide vital information about the genetic health and other abnormalities of a fetus and poses no considerable risk for the fetus would be invaluable.[2] The prenatal diagnosis provides an opportunity for physicians to identify causes and to evaluate corrective interventions and helps the parents by giving them enough time to emotionally and mentally cope with fetal health status and selection of possible clinical options.[2,3] Prenatal diagnostic methods are constantly evolving.[4] Amniocentesis (at 12 to 14 weeks' gestation) and chorionic villus sampling (CVS) (at 9 to 10 weeks' gestation) are at present the only reliable methods of prenatal diagnosis. Although both these procedures are highly sensitive and accurate, unfortunately, due to their invasiveness, they carry the risk of abortion and fetal structural deformities, even in experienced hands, and are usually performed at stages of pregnancy where clinical options are limited for parents and physicians.[5–7] Therefore, in recent decades, attention has been focused on the developing of a noninvasive highly reliable method that would be feasible in the early stages of pregnancy.[8,9] Currently, the noninvasive cell-free fetal DNA (cffDNA) method, despite its limitations, such as the low percentage and the fragmented nature of fetal DNA in maternal plasma, the associated problems in their separation and analysis, under the influence of gestational age and maternal weight and available after the first ten weeks of gestation are used for prenatal screening. Due to the limitations of the cffDNA method, an alternative NIPT method is necessary.[10–15] Recently, the retrieval of trophoblast cells from the cervix has attracted attention from scientists as a potential source of fetal DNA for prenatal diagnosis.[15] In 1971, Shettles first observed the shedding and presence of trophoblast cells in the uterus and cervix.[16] The first embryonic lineage that differentiates during fetal development for forming the placenta is trophoblast cells. Trophoblast cells contain two main lineages, villous trophoblast (VT) and

[a]Department of Genetics, Faculty of Medicine, Shahid Sadoughi University of Medical Sciences and Health Services, Yazd, 8916978477, Iran. E-mail: smkalantar38@gmail.com; smkyzd@gmail.com

[b]Department of Chemistry, University of Isfahan, Isfahan, 81746-73441, Iran

[c]California Institute for Quantitative Biosciences (QB3), University of California, Berkeley, CA 94720, USA

[d]Department of Medicinal Chemistry, Faculty of Pharmacy and Pharmaceutical Sciences Research Centre, Shahid Sadoughi University of Medical Sciences and Health Services, Yazd, 8916978477, Iran

[e]Department of Immunology, Faculty of Medicine, Shahid Sadoughi University of Medical Sciences and Health Services, Yazd, 8916978477, Iran

[f]Department of Biotechnology, Faculty of Biological Science and Technology, University of Isfahan, Isfahan, 81746-73441, Iran

[g]Research and Clinical Centre for Infertility, Yazd Reproductive Sciences Institute, Shahid Sadoughi University of Medical Sciences, Yazd, 8916978477, Iran

† These authors contributed equally to this work.

© 2021 The Author(s). Published by the Royal Society of Chemistry

Open Access Article. Published on 20 September 2021. Downloaded on 11/9/2025 1:16:10 AM.
This article is licensed under a Creative Commons Attribution-NonCommercial 3.0 Unported Licence.

extravillous trophoblast (EVT), with different functions. EVT cells differentiate wherein the placenta contacts with the uterine decidua.[17,18] Some of them are shed into the reproductive tract from diverse invasive routes and then are trapped in the transcervical mucus and can be retrieved from the endocervical canal in ongoing pregnancies by a cytobrush.[15,19] The possibility of capturing the intact fetal EVT cells from the endocervical canal provides a noninvasive alternative for early prenatal diagnosis.[10] The number of EVTs in cytobrush-retrieved endocervical samples from pregnancy is approximately 1 EVT cell in 2000 maternal cervical cells.[19] The major challenge of using EVTs for the evaluation of prenatal screening is the inability to efficiently isolate them from maternal cells.[19] The presence of different antigens (Ags) in trophoblast cells from maternal cervical cells provides the potential to isolate these cells by Ag-based methods.[2,20–22] In recent years, attempts at cell isolation by conventional methods of magnetic cell sorting (MACS) and fluorescence-activated cell sorting (FACS) have been reported.[23] However, the development of an isolation method with a minimal technical challenge, high separation ability and clinical applicability is still needed.[24] Both MACS and FACS isolation methods are dependent on the specific cell surface marker that can be distinguished by magnetic microbead or fluorescent-tagged antibody (Ab).[25] Considering FACS is a sophisticated, time-consuming and expensive technique that is not suitable for clinical use. On the other hand, studies show that the MACS method is a powerful, fast and simple strategy for cell isolation and is more cost-effective and time-saving.[26] Accordingly, the present study describes a magnetic force-based platform for the isolation of fetal cells.

Magnetic nanoparticles (MNPs), due to their special properties including the availability of functional groups for chemical modification, biocompatibility and easy separation from the reaction mixture by use of magnet are a proper immobilization support of bio-macromolecules for magnetic separation.[27–30] The smaller nanoparticles (NPs) have the higher surface to volume ratio causing greater binding capacity for ligand and greater separation efficiency.[31] Because of the multiple-point attachment, cell separation with large magnetic particles is difficult and they aggregate due to too magnetic and cells get nonspecifically trapped in the aggregates.[26] The use of MNPs for separation requires precise physicochemical design and unique targeting.[32,33] Iron oxide (Fe_3O_4) NPs have application potential as a support in magnetic separation owing to their strong superparamagneticity, biocompatibility, low cytotoxicity, simple preparation process, having surface hydroxyl groups for modification and low cost.[34] Despite all the advantages, the naked Fe_3O_4 NPs are unstable and oxidize easily in the air or aqua fluid and their magnetic properties and dispersion reduce.[35,36] Therefore, the introduction of an outer shell is very important to maintain the stability of Fe_3O_4 NPs.[37] Fe_3O_4 NPs are usually coated with various shells such as silica (SiO_2), Au, dextran, albumin or polyethylene glycol.[35,38] The incorporation of a silica coating is an efficient and appropriate strategy to improve the stability and dispersion of Fe_3O_4 NPs.[39] On the other hand, chemistry of silica is well known and can be conjugated with different functional groups for various biochemical and biomedical purposes.[35] In order to isolate rare target cells from a sample, target cell-specific antibody conjugation to the surface of the magnetic NPs is commonly used due to the remarkable binding affinity and specificity between Ab and Ag.[40,41] EVT cells can be isolated from the endocervical sample by binding appropriate antibodies to MNPs. Human leukocyte antigen-G (HLA-G) is an EVT-specific Ag and by targeting this specific Ag, EVT cells can be isolated from cervical cells.[19,42] The MEM-G/9 antibody shows a strong affinity towards the native form of human HLA-G.[43,44] There are five basic methods of Ab immobilization onto NPs: physical adsorption, ionic interaction, and covalent bond, through protein cofactor and by antibody disulfide bond cleavage. Covalent bonding can stably bind Abs onto NPS, which is vital to the immobilization of the Abs in order for them to be used in the isolation process.[45,46] The covalent attachment of Abs to the NPs surface generally requires the surface modifications of NPs.[47] Thus, the silica-coated magnetite nanoparticles were modified by 3-aminopropyl triethoxysilane (APTES) to introduce the amine groups and then by 2,4,6-trichlorotriazine (TCT) to introduce the chlorine functional group. TCT is an important linker for the immobilization of biomolecules due to its low cost, biocompatibility, and chemoselective reactivity.[36] TCT leads to conjugating NPs with antibody amine groups.[47] In accordance with existing amine groups in most proteins and their high reactivity, this method does not require chemical manipulation of the antibody structure.[48] In the present study, synthesized Fe_3O_4@SiO_2-APTES-TCT nanoparticles were conjugated with MEM-G/9 antibody by direct and indirect methods and then their function in HLA-G^+ cells isolation was evaluated. The successful isolation of HLA-G^+ cells has provided an opportunity to assess the genetic health of fetus and investigate the placenta function.

2 Experimental

2.1 Materials

All the chemical reagents were commercially purchased and used without further purification. Ferric chloride hexahydrate ($FeCl_3 \cdot 6H_2O$, ≥99%), ferrous chloride tetrahydrote ($FeCl_2 \cdot 4H_2O$, ≥99%), ethanol (96%), ammonium hydroxide (NH_4OH, 25%), hydrochloric acid (HCl, 37%), toluene (99.8%), triethylamine (TEA, ≥99.5%), trichlorotriazine (TCT, 99%), acetone (≥99.8%), di-sodium hydrogen phosphate (Na_2HPO_4, ≥99%), sodium phosphate monobasic (NaH_2PO_4, ≥99%), sodium chloride (NaCl, ≥99.5%), acetic acid (glacial, 100%), and sodium acetate (≥99%) were provided by Merck company (Germany). 3-Aminopropyl triethoxysilane (APTES, ≥98%), tetraethyl orthosilicate (TEOS, 98%), diisopropylethylamine (DIPEA, ≥98%), bovine serum albumin (BSA, ≥96%) and 1% penicillin–streptomycin were obtained from Sigma Aldrich (Germany). Tetrahydrofuran (THF, >99%) was purchased from Duksan (Korea). Bovine γ-globulin (BGG, 99%) and the Bradford reagent were bought from Bio-Rad (USA). The human breast cancer cell line SK-BR-3 and the human choriocarcinoma cell line JEG-3 were purchased from Pasteur Institute of Iran (Tehran, Iran). Fetal bovine serum (FBS), trypsin–EDTA (0.05%) and RPMI-1640 was obtained from Gibco (UK). The DMEM/F12

Open Access Article. Published on 20 September 2021. Downloaded on 11/9/2025 1:16:10 AM.
This article is licensed under a Creative Commons Attribution-NonCommercial 3.0 Unported Licence.

medium was acquired from Bio-Idea (Iran). Also, the purified monoclonal MEM-G/9 antibody (Exbio, Czech Republic), the FITC goat anti-mouse (IgG) secondary antibody (ab6785, Abcam, Cambridge, MA), the goat anti-mouse antibody (ab6708, Abcam, Cambridge, MA), the fluorescent dye propidium iodide (PI) (Fluka, 81845, Switzerland), the fluorescent dye 4′,6-diamidino-2-phenylindole (DAPI, Cytocell, UK) and phosphate buffered saline (PBS, pH 7.4, Inoclon) were used in this study. Deionized (DI) water was prepared with ultrapure water system (Easy Pure II, 18.2 MΩ, Barnstead Co).

2.2 Synthesis of Fe_3O_4@SiO_2-APTES-TCT

The whole process of synthesis of 1,3,5-triazine functionalized silica-coated iron oxide NPs and the immobilization of MEM-G/9 antibody on MNPs are described here and are shown schematically in Fig. 1.

2.2.1 Synthesis of iron oxide (Fe_3O_4) NPs. The superparamagnetic iron oxide nanoparticles were synthesized by the co-precipitation approach.[49–52] Briefly, a solution containing 3 g of $FeCl_2 \cdot 4H_2O$ and 8.5 g of $FeCl_3 \cdot 6H_2O$ in 38 ml of 0.4 M HCl was prepared. The mixture was quickly dropped into 375 ml of 0.7 M NH_4OH solution at 45 °C under argon atmosphere and vigorous stirring *via* the combination of mechanical stirring and ultrasonic vibration. The solution colour changed from pale yellow to black. The reaction was maintained at about 45 °C under argon for 30 min. After 30 min and cooling the solution, the resulting black precipitate was sedimented by an external magnet and washed three times with deionized water and once with ethanol and finally dried in a vacuum oven for 24 h at room temperature.

2.2.2 Surface coating of Fe_3O_4 NPs with silica (Fe_3O_4@SiO_2 NPs). For preservation of Fe_3O_4 NPs from aggregation and oxidation, their surfaces were coated with the silica. 0.725 g of Fe_3O_4 NPs was ultrasonically and mechanically dispersed in 200 ml of ethanol under argon at room temperature for 40 min. Then 30 ml of deoxygenated deionized water, 15 ml of 25% ammonium hydroxide and 2 ml of TEOS were added to the solution under vigorous stirring. Afterward, the mixture solution was further stirred for 5 h at room temperature. After completion of the reaction, the Fe_3O_4@SiO_2 nanoparticles were collected by an external magnet and washed with water, ethanol and acetone and dried in a vacuum oven at room temperature.[53]

2.2.3 Functionalization of Fe_3O_4@SiO_2 NPs by APTES. The functionalization of Fe_3O_4@SiO_2 NPs by APTES created amine groups on their surface that was then reacted with TCT. The Fe_3O_4@SiO_2-APTES NPs were prepared according to the procedure reported by Hou *et al.* with slight modifications.[54] 0.4 g vacuum-dried Fe_3O_4@SiO_2 was dispersed in 180 ml dried toluene for 30 min. Afterward, 6 ml of APTES and 2 ml of TEA were added into the reaction mixture and it was refluxed at 70 °C under nitrogen atmosphere for 24 h with continuous stirring. After cooling down the reaction to room temperature, the obtained amino-functionalized Fe_3O_4@SiO_2 NPs were collected using an external magnetic field and washed successively with toluene, ethanol and acetone and dried. Finally, NPs were dried in a vacuum oven at 60 °C overnight.

2.2.4 Modification process of Fe_3O_4@SiO_2-APTES NPs using TCT. The surface of Fe_3O_4@SiO_2-APTES NPs was modified by TCT to generate a triazine modified surface for antibody immobilization. For the preparation of the Fe_3O_4@SiO_2-APTES-TCT NPs, to a dispersion of 0.5 gr Fe_3O_4@SiO_2-APTES NPs in 40 ml dried THF were added 0.25 gr TCT and 1 ml DIPEA. The solution was mechanically stirred at 0 °C for 6 h under nitrogen atmosphere. The modified NPs (Fe_3O_4@SiO_2-APTES-TCT) were separated with a magnet and washed with THF and acetone and then dried in a vacuum oven at room temperature.[55]

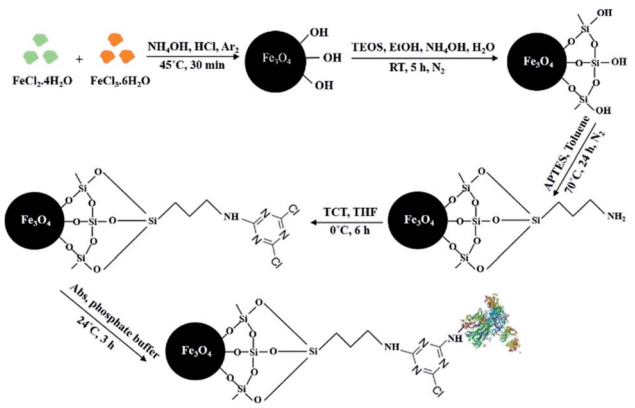

Fig. 1 Schematic diagram of the synthesis route of the antibody immobilization on triazine-functionalized magnetic nanoparticles. Abs: antibodies, APTES: 3-aminopropyl triethoxysilane, TCT: trichlorotriazine, TEOS: tetraethyl orthosilicate, THF: tetrahydrofuran.

2.3 Immobilization of anti-HLA-G MEM-G/9 Ab onto Fe_3O_4@SiO_2-APTES-TCT NPs

2.3.1 Direct immobilization of MEM-G/9 Ab. At first, 1 mg of the triazine functionalized MNPs were dispersed in 1 ml of 150 mM phosphate buffer (pH 8.5) with 150 mM NaCl under ultrasonication for 5 min. Then three amounts of MEM-G/9 Ab (5, 10 and 20 μg) were added to the 180 μl dispersed NPs and the mixture was shaken gently to avoid sedimentation of the NPs at 24 °C for 4 h. In order to remove the non-bound Abs, NPs were magnetically collected and washed twice with phosphate buffer (ESI Fig. 1†). The non-bound Ab amount in the supernatant was quantified with Bradford protein assay using BGG as the standard protein. The initial optimal Ab amount according to the immobilization percentage of Ab and the ratio of the immobilized amount of Ab to 0.18 mg MNPs was obtained. The immobilized amount of Ab on MNPs was calculated based on the difference between the Ab amount before and after immobilization. The immobilization percentage of Ab was obtained from eqn (1):

$$\text{Immobilization (\%)} = [(C_i - C_s)/C_i] \times 100 \quad (1)$$

C_i and C_s are the concentrations of initial Ab and non-bound Ab in the supernatant, respectively.

2.3.2 Indirect immobilization of MEM-G/9 Ab. A two-step of incubation was used for indirect immobilization. At first, the range of 2 to 60 μg goat anti-mouse IgG Ab was added to 180 μl of dispersed NPs and the mixture was shaken slowly at 24 °C for 4 h. The supernatant of each sample was separated with an

 © 2021 The Author(s). Published by the Royal Society of Chemistry

Open Access Article. Published on 20 September 2021. Downloaded on 11/9/2025 1:16:10 AM.
This article is licensed under a Creative Commons Attribution-NonCommercial 3.0 Unported Licence.

external magnet to measure non-bond Ab with Bradford protein assay and the initial optimal IgG Ab amount was obtained. Then, IgG-MNPs (with initial optimal amount) were added into the tube containing cells labeled with MEM-G/9 Abs and incubated for 1 h at 37 °C with mixing (ESI Fig. 2†).

2.4 Characterization methods

Fourier infrared spectroscopy (FTIR, PerkinElmer, Spectrum Two, USA), transmission electron microscope (TEM, Philips, CM120, Netherlands), energy dispersive X-ray spectroscopy (EDS, TESCAN, model MIRA III, Czech Republic), zeta potential (Zetasizer Nano-ZS, model Zen3600, Malvern Instrument Ltd, Malvern, UK) and vibrating sample magnetometer (VSM, Quantum Design, USA) were utilized to analyse the certain functional groups, morphology, size, elemental composition, electrical charge and magnetic properties of modified MNPs. Thermogravimetric analysis (TGA) was performed to confirm immobilization of Ab on MNPs using a TA Q600 (USA) from 30 to 600 °C at 10 °C min^{-1} heating rate in air atmosphere.

2.5 Optimization of immobilization time

20 μl of goat anti-mouse IgG Ab (1 mg ml^{-1}) was added to 180 μl of the dispersed triazine functionalized MNPs in phosphate buffer. The mixture was shaken at 24 °C for 0.25–16 h. The amount of IgG immobilized on MNPs was quantified by Bradford assay.

2.6 Confirmation of immobilization of HLA-G Ab with the immune reactivity

The immobilization of HLA-G Abs onto the modified MNPs was investigated by the following procedure. At first, 20 μg of MEM-G/9 Ab was added to 180 μl of dispersed MNPs (1 mg ml^{-1}), incubated at 24 °C for 3 h and washed with PBS to remove any unconjugated Ab. The MEM-G/9-immobilized MNPs were blocked with 1% BSA for 2 h. Then, goat anti-mouse IgG H&L (FITC), a secondary antibody, was used to recognize the immobilization and the immune reactivity of MEM-G/9 Ab conjugated to the MNPs surface. 200 μl of FITC anti-IgG (50 μg ml^{-1}) was added to the BAS blocked MEM-G/9-MNPs and the resulting mixture was incubated at 24 °C for 2 h. After complete washing with PBS, the collected MNPs were redispersed in 100 μl PBS and immobilized on glass slide by cytospin centrifugation for 5 min, 1500 rpm for examination under a microscope (ESI Fig. 3†).

2.7 Cell culture

The human HLA-G-positive JEG-3 trophoblast tumor cells[56–58] were cultured in a 1 : 1 mixture of Dulbecco's Modified Essential Medium and Ham's F-12 Medium (DMEM/F12 Medium) supplemented with 10% (v/v) inactivated FBS and 1% (v/v) streptomycin/penicillin. SKBR-3 cells with reduced or absent expression of HLA-G gene[59–61] were grown in RPMI 1640 medium containing 10% FBS and 1% penicillin/streptomycin.

2.8 Quality assessment of the immobilized Ab on the MNP surface by experiment of cell binding

To show that the Ab-MNPs (Ab-conjugated MNPs) are able to target cells when JEG-3 cells have reached the desired number on the coverslip, the culture media was removed and washed gently with PBS. Then, the cells cultured on each coverslip were fixed at room temperature with a mixture of acetate buffer and methanol for 15 min. After washing, cells were blocked with 3% BSA–PBS for 45 min at room temperature. In the case of nanoparticles conjugated directly to MEM-G/9, 50 μl of these nanoparticles were added to the blocked cells. Triazine functionalized MNPs without MEM-G/9 were used as control. The cells were incubated with MNPs (with or without Ab) at 37 °C for 1 h. The coverslip was carefully removed with forceps from the culture plate. It was inverted and placed on a glass slide and examined by light microscope. In the case of nanoparticles conjugated indirectly to MEM-G/9, at first, the blocked cells were incubated with MEM-G/9 (at 1 : 50 dilution in 1% BSA–PBS) at 37 °C for 1 h. Subsequently, 50 μl of IgG-MNPs were added to the cells and incubated at 37 °C for 1 h. The incubated cells with the antibody diluent alone and no MEM-G/9 Ab were used as control.

2.9 Showing the ability of Ab-MNPs to capture the JEG-3 cells

About 5×10^5 JEG-3 cells as target cells were poured into a tube and fixed with a mixture of acetate buffer and methanol for 15 min. The cells were centrifuged at 1400 rpm for 7 min and blocked with 3% BSA–PBS for 45 min at room temperature. In the case of nanoparticles conjugated directly to MEM-G/9, the blocked cells were incubated with 50 μl of MEM-G/9-MNPs at 37 °C for 1 h with shaking and were separated by an external magnetic field. After magnetic separation, the number of cells in the supernatant was counted to know the capture efficiency of the Ab-MNPs. The average capture efficiency was obtained according to the results of three experiments.

$$\text{Capture efficiency (\%)} = ((\text{initial JEG-3 cells} - \text{supernatant JEG-3 cells})/\text{initial JEG-3 cells}) \times 100$$

In the case of nanoparticles conjugated indirectly to MEM-G/9, first, the cell suspension was incubated with MEM-G/9 at 37 °C for 1 h. Subsequently, 50 μl of IgG-MNPs were added to the cells and incubated at 37 °C for 1 h with shaking. All subsequent steps were identical to those described above.

2.10 Detection and isolation of HLA-G^+ cells using Ab-MNPs

To display the capability of Ab-MNPs for HLA-G-positive cells isolation, JEG-3 cells were utilized as HLA-G-positive cells and SK-BR-3 cells were utilized as HLA-G-negative cells. The fixed and blocked JEG-3 cells (about 5×10^5) were stained with DAPI dye (blue) and the fixed and blocked SK-BR-3 cells (about 5×10^5) were stained with Propidium iodide (PI) dye (red). After staining, cells were mixed together. In the case of nanoparticles conjugated directly to MEM-G/9, 50 μl of MEM-G/9-MNPs was added to the mixed cells and incubated for 60 min at 37 °C in the dark. The mixture was vortexed every 15 min. After incubation, the mixture was kept in front of a magnet for 10 min to allow magnetic isolation of the cells + MEM-G/9-MNPs. Both the supernatant and the pellet were carefully collected. The pellet was resuspended in 50 μL PBS. Then, the pellet and the

Open Access Article. Published on 20 September 2021. Downloaded on 11/9/2025 1:16:10 AM.
This article is licensed under a Creative Commons Attribution-NonCommercial 3.0 Unported Licence.

supernatant were immobilized on glass slide and examined with a fluorescence microscopy (BX61, Olympus, Tokyo, Japan) connected to Applied Spectral Imaging (ASI) Acquisition 5.5 software (ASI Inc, Carlsbad, CA). In the case of nanoparticles conjugated indirectly to MEM-G/9, first, the mixed cells were incubated with MEM-G/9 at 37 °C for 1 h. Afterward, 50 μl of IgG-MNPs was added to the cells and incubated at 37 °C for 1 h. All subsequent steps were identical to those described above.

3 Results and discussion

3.1 Fe_3O_4@SiO_2-APTES-TCT synthesis

At present, the isolation of target cells from heterogeneous cell populations is important for various biomedical purposes. Methods for isolation and enrichment of cells are evolving. A simple, accurate and inexpensive method that achieves acceptable results in the shortest amount of time possible has been one of the important research goals of scientists in recent years. The magnetic isolation of cells is one of the most appropriate approaches for separating target cells. The magnetic isolation method usually uses MNPs conjugated with antibodies against specific cell surface Ags. Therefore, the synthesis of immunomagnetic nanoparticles using a simple, cost-effective and high-performance method is a critical step for cell isolation. In this study, magnetic nanoparticles were synthesized by the simple and fast co-precipitation method and coated with silica shell for improving their stability. The silica-coated MNPs were then modified through a two-step process with APTES and 2,4,6-trichloro-1,3,5-triazine to create a functional surface with triazine to immobilize the antibody and several techniques were used to characterize them.

3.2 Antibody immobilization on MNPs

Fe_3O_4@SiO_2 NPs were functionalized with triazine to enable subsequent covalent bond *via* the amine groups of antibodies. The amount of immobilized antibody was determined according to the linear equation obtained from the BGG standard curve (ESI Fig. 4†).

3.2.1 Optimal initial amount of MEM-G/9 for immobilization on MNPs. The amount of immobilized MEM-G/9 on MNPs and the immobilization percentage in the different initial amounts of MEM-G/9 were estimated and the results were shown in Fig. 2A. As can be seen in the figure, the amount of immobilized Ab rose with increasing the initial amount of MEM-G/9, while the immobilization percentage decreased simultaneously. The initial amount of Ab was low at first and all the initial amount was immobilized on MNPs. Then, although

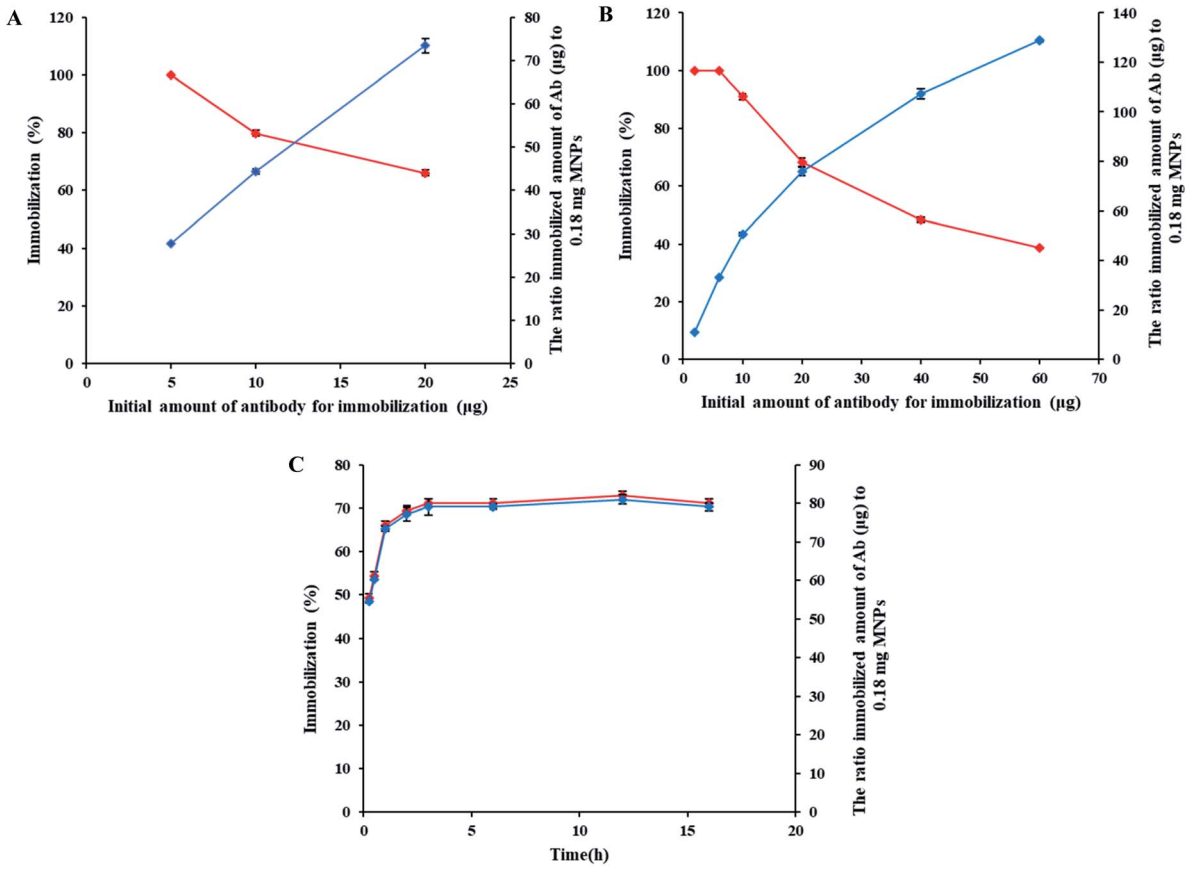

Fig. 2 (A) Effect of the initial amount of HLA-G antibody on immobilization percentage (the red graph) and amount of immobilized antibody on nanoparticles (the blue graph). (B) Effect of the initial amount of anti-mouse IgG antibody on immobilization percentage (the red graph) and amount of immobilized antibody on nanoparticles (the blue graph). (C) Effect of reaction time on the immobilization percentage (the red graph) and amount of immobilized antibody on nanoparticles (the blue graph).

 © 2021 The Author(s). Published by the Royal Society of Chemistry

Open Access Article. Published on 20 September 2021. Downloaded on 11/9/2025 1:16:10 AM.
This article is licensed under a Creative Commons Attribution-NonCommercial 3.0 Unported Licence.

by increasing the initial amount, more antibodies were immobilized onto the surface area, but probably due to the decrease in the TCT active sites, the ratio of immobilized Abs to the total initial Abs as immobilization percentage decreased. Given that in this study, the immobilization Ab is random and adverse orientation can occur. To increase the likelihood of having active Ag-binding sites, the maximum initial amount of MEM-G/

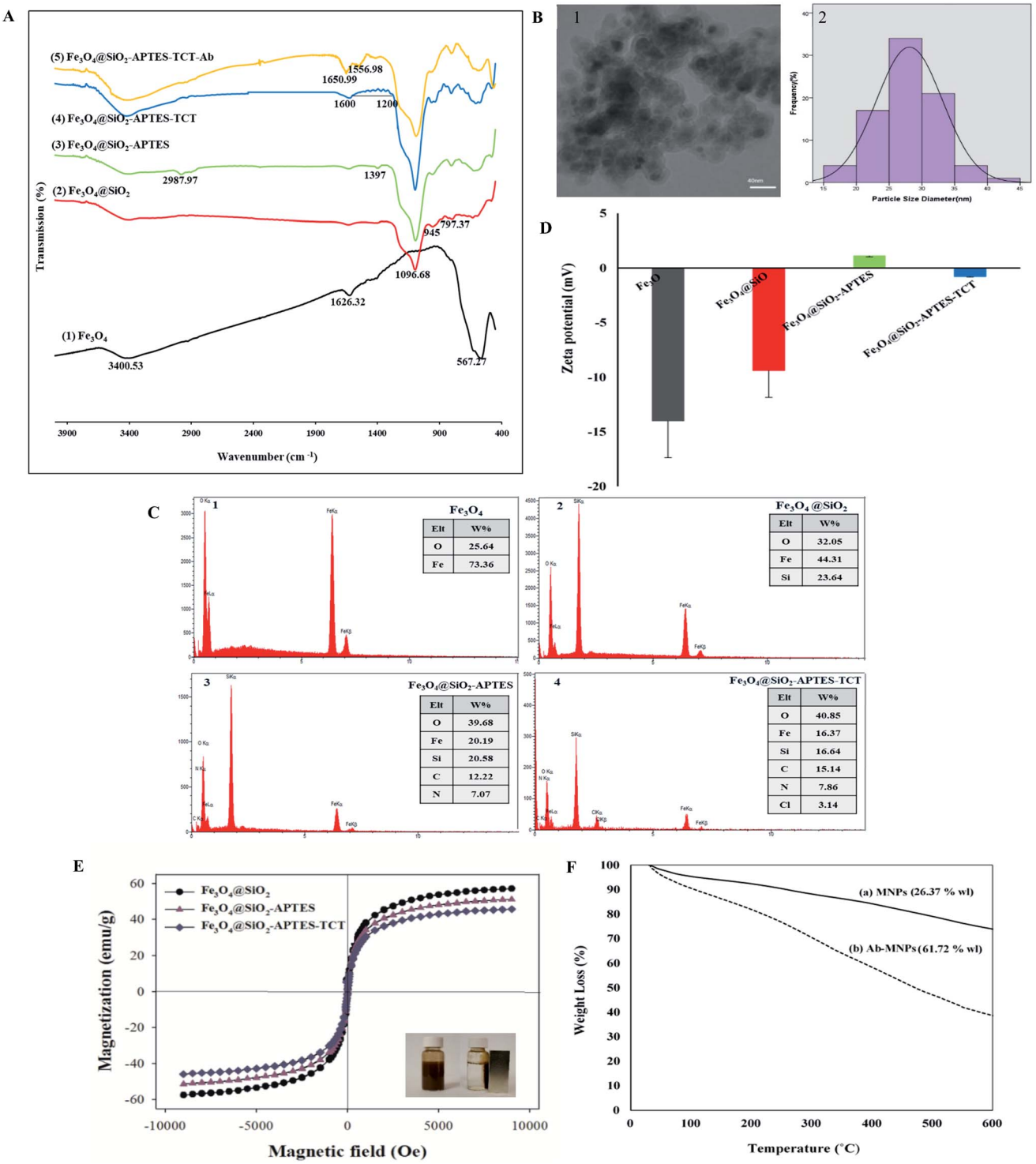

Fig. 3 Characterization of MNPs and Ab-MNPs. (A) The FTIR spectra of (1) Fe_3O_4, (2) Fe_3O_4@SiO_2, (3) Fe_3O_4@SiO_2-APTES, (4) Fe_3O_4@SiO_2-APTES-TCT and (5) Fe_3O_4@SiO_2-APTES-TCT-Ab nanoparticles. (B) The TEM image (1) and size distribution histogram (2) of Fe_3O_4@SiO_2-APTES-TCT nanoparticles. (C) The EDX spectrum of (1) Fe_3O_4, (2) Fe_3O_4@SiO_2, (3) Fe_3O_4@SiO_2-APTES and (4) Fe_3O_4@SiO_2-APTES-TCT. (D) The Zeta potential analysis of Fe_3O_4, Fe_3O_4@SiO_2, Fe_3O_4@SiO_2-APTES and Fe_3O_4@SiO_2-APTES-TCT. (E) Room temperature magnetization curves of Fe_3O_4@SiO_2 (●), Fe_3O_4@SiO_2-APTES (▲) and Fe_3O_4@SiO_2-APTES-TCT (◆). (F) The TGA spectra of (a) Fe_3O_4@SiO_2-APTES-TCT and (b) Ab-MNPs.

Open Access Article. Published on 20 September 2021. Downloaded on 11/9/2025 1:16:10 AM.
This article is licensed under a Creative Commons Attribution-NonCommercial 3.0 Unported Licence.

9 (20 μgr) with conjugation efficiency of 66.1% as the optimal amount was chosen for immobilization.

3.2.2 Optimal initial amount of anti-mouse IgG for immobilization on MNPs. The amount of immobilized anti-mouse IgG on MNPs and the immobilization percentage in the studied concentration range was illustrated in Fig. 2B. According to the results, for the balance of cost and immobilization efficiency, 20 μgr of anti-mouse IgG (with conjugation efficiency of 68.36%) was selected as the optimum initial amount of anti-mouse IgG.

3.3 Characterization of MNPs and Ab-MNPs

3.3.1 FTIR of MNPs and Ab-MNPs. The FT-IR spectra of Fe_3O_4, $Fe_3O_4@SiO_2$, $Fe_3O_4@SiO_2$-APTES, $Fe_3O_4@SiO_2$-APTES-TCT and $Fe_3O_4@SiO_2$-APTES-TCT-Ab NPs were taken in the range of 400 to 4000 cm^{-1} and presented in Fig. 3A. In Fe_3O_4 spectra, the strong peak at 567.27 cm^{-1}, related to Fe–O bond bending vibration, confirmed the formation of MNPs. Two absorption peaks at 1626.32 and 3400.53 cm^{-1} are due to the presence of hydroxyl groups at the Fe_3O_4 surface. The peaks at 797.37, 945 and 1096.68 cm^{-1} in $Fe_3O_4@SiO_2$ spectra were associated with the symmetric stretching Si–O–Si vibration, Si–OH bending vibration and asymmetric stretching Si–O–Si, respectively.[62] The Fe–O–Si peak cannot be clearly identified in the FTIR spectrum because it is at about 584 cm^{-1} and overlaps with the Fe–O peak of MNPs.[63] The obtained results confirmed the presence of silica coating on the surface of Fe_3O_4 NPs. The functional process of $Fe_3O_4@SiO_2$ with APTES was confirmed by the presence of peaks at 2987.97 and 1397 cm^{-1} corresponding to C–H stretching vibration and C–H scissoring vibration, respectively.[64] However, two peaks at around 3450 and 1640 cm^{-1} related to NH_2 vibrations cannot be observed due to the weak dipole moment of the amine groups.[65–67] The peaks between 1000 and 1600 cm^{-1} in $Fe_3O_4@SiO_2$-APTES-TCT spectra can be ascribed to the C–N and C=N stretching vibrations which prove the presence of triazine rings onto MNPs.[68,69] In $Fe_3O_4@SiO_2$-APTES-TCT-Ab spectra, two absorption peaks at 1556.98 cm^{-1} (N–H stretching vibration of antibody amide II) and 1650.99 cm^{-1} (C=O stretching vibration and antibody amide I) confirmed the success of Ab immobilization on modified MNPs.[47,70]

3.3.2 TEM of $Fe_3O_4@SiO_2$-APTES-TCT NPs. TEM images of $Fe_3O_4@SiO_2$-APTES-TCT NPs (Fig. 3B1) displayed that the particles were quasi-spherical with a size distribution ranging from 15–45 nm and an average of 28.10 ± 5.06 nm (Fig. 3B2). The distribution of particle size was characterized by randomly measuring the diameter of around 100 nanoparticles using ImageJ software. Because the particles were much smaller than a cell (10–100 μm),[71] many of them were able to make effective contact with the cell surface and prevented the cells from fragmenting while isolated,[72] but they agglomerated due to their small size and high reactivity.[35] The silica coating thickness was also found in a range between 3.5 and 6.3 nm and an average of 5.12 ± 0.863 nm (data not shown). If the silica coating thickness in the core–shell MNPs increases; results in the reduction in their magnetization in the magnetization field and in the quantity of the immobilized biomolecules.[48,73–75]

3.3.3 The findings of EDAX analysis. The accuracy of each synthesis step was confirmed by EDAX analysis of products: Fe_3O_4, $Fe_3O_4@SiO_2$, $Fe_3O_4@SiO_2$-APTES, and $Fe_3O_4@SiO_2$-APTES-TCT. EDAX pattern of the Fe_3O_4 NPs displayed the presence of both iron and oxygen (Fig. 3C1). For each product, iron and oxygen elements were identified as a result of the Fe_3O_4 structure. In Fig. 3C2, the presence of a strong silica peak and the remarkable reduction of Fe peak verified the silica coating on the surface of Fe_3O_4 NPs. In Fig. 3C3, N and C elements appeared after the surface modification of MNPs, suggesting successful modification of the MNPs with APTES. In Fig. 3C4, the chlorine peak appeared and the content of N and C elements increased. These results indicated that MNPs were modified with TCT successfully.

3.3.4 Zeta potential (ζ). The zeta potential of Fe_3O_4, $Fe_3O_4@SiO_2$, $Fe_3O_4@SiO_2$-APTES, and $Fe_3O_4@SiO_2$-APTES-TCT NPs was −14 ± 3.36 mV, −9.37 ± 2.48 mV, 1.13 ± 0.1 mV and −0.771 ± 0.05 mV, respectively (Fig. 3D). The negative charges of Fe_3O_4 and $Fe_3O_4@SiO_2$ NPs were due to the presence of hydroxyl (OH) and silanol (Si–OH) groups on their surface.[76–78] After modification, the zeta potential of the $Fe_3O_4@SiO_2$-APTES NPs increased to 1.13 mV compared to the $Fe_3O_4@SiO_2$ NPs because of the presence of positively charged amino groups onto the surface of $Fe_3O_4@SiO_2$ NPs.[79] In contrast, the zeta potential of $Fe_3O_4@SiO_2$-APTES NPs changed to approximately −0.771 mV due to the presence of triazine rings after functionalization with TCT. The zeta potential changes also confirmed the successful preparation of the functionalized MNPs.

3.3.5 VSM. The magnetic properties of $Fe_3O_4@SiO_2$, $Fe_3O_4@SiO_2$-APTES, and $Fe_3O_4@SiO_2$-APTES-TCT NPs *versus* magnetic field at ambient temperature were investigated by VSM and shown in Fig. 3E. Their saturation magnetization (M_s) was 58, 50, and 45 emu g^{-1}, respectively.

Three magnetization curves showed superparamagnetic behaviour due to the lack of hysteresis.[80] As can be seen in Fig. 3E, $Fe_3O_4@SiO_2$ NPs indicated a slightly higher level of Ms than other MNPs. The decrease of Ms in $Fe_3O_4@SiO_2$-APTES, and $Fe_3O_4@SiO_2$-APTES-TCT NPs was due to the modification of MNPs with aminopropyl[81] and triazine groups and the increase in the total mass with respect to the magnetic material.[55] However, the modifications have had little effect on the magnetization of the MNPs and can be quickly separated from the solution by an external magnet.[80]

3.3.6 TGA. The antibody immobilization on MNPs was also confirmed with TGA analysis. TGA results usually represent a two-stage thermal decomposition profile from the sample. The first stage of weight loss (wl) in the temperature range below 200 °C is attributed to removal of physically adsorbed water and organic solvents and the second main stage of weight loss is at temperatures higher than 200 °C to decompose surface organic functional groups and surface-bound biomolecules.[36,47] The weight loss plots of the MNPs and Ab-MNPs showed a two-step thermal decomposition (Fig. 3F). The difference in weight loss between the MNPs and Ab-MNPs (35.35% wl) in the temperature range between 200 and 600 reflected the antibody immobilization on the surface of the MNPs.

 © 2021 The Author(s). Published by the Royal Society of Chemistry

Open Access Article. Published on 20 September 2021. Downloaded on 11/9/2025 1:16:10 AM.
This article is licensed under a Creative Commons Attribution-NonCommercial 3.0 Unported Licence.

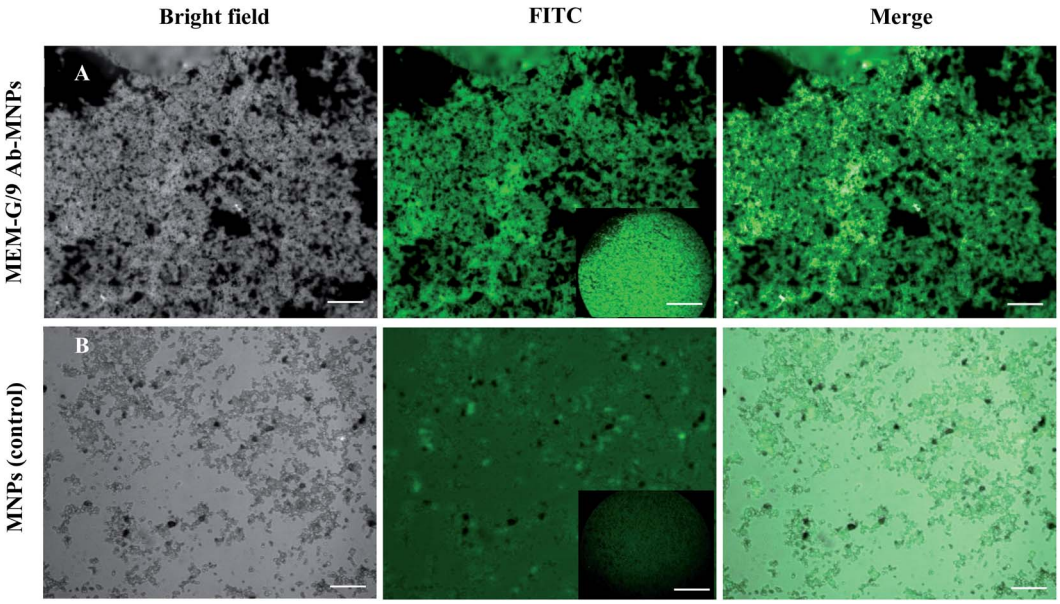

Fig. 4 The fluorescent microscopy images of the reactivity of immobilized MEM-G/9 antibodies on Fe_3O_4@SiO_2-APTES-TCT nanoparticles with the FITC-labeled IgG secondary antibodies (A) and the reactivity of BSA-blocked nanoparticles without MEM-G/9 antibody conjugation (control) with the FITC-labeled IgG secondary antibody (B). Scale bars = 5 μm, 1000× magnification.

3.4 Effect of immobilization time

Fig. 2C shows the results of the amount of immobilized anti-mouse IgG on MNPs and the immobilization percentage in various reaction times. The amount of immobilized Ab and the immobilization percentage reached their maximum after 3 h and then remained constant, and further elongation of reaction time did not significantly increase the amount and percentage of antibody immobilization. That was probably because there was no free TCT active group left to connect with the Ab amine groups and consequently more immobilization after 3 h.[82] Therefore, 3 h was considered as the optimal time for Ab immobilization.

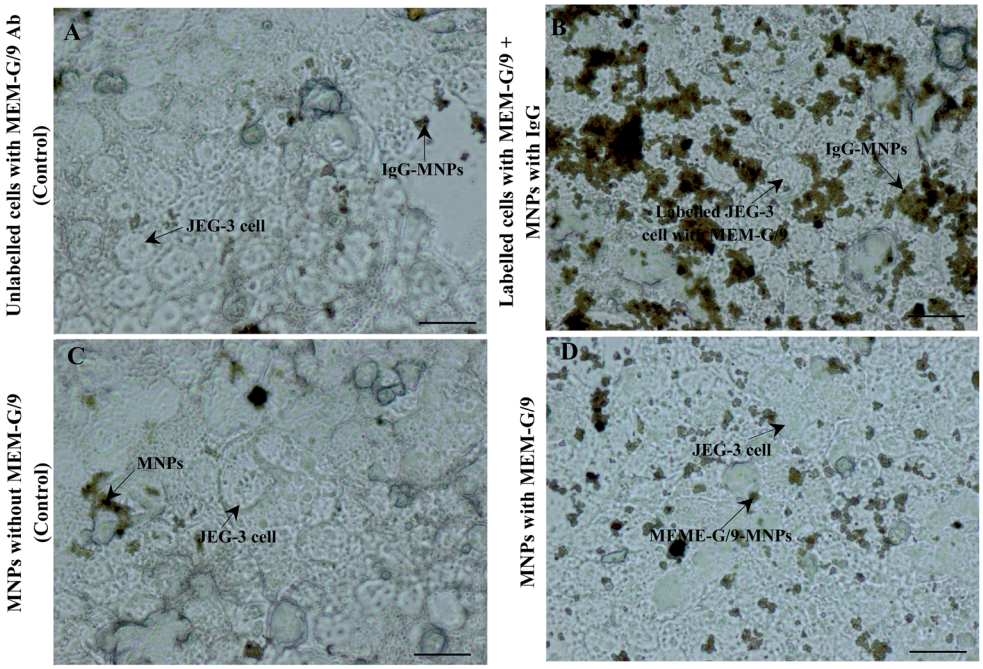

Fig. 5 The light microscopy images of Ab-MNPs tendency to be HLA-G-positive JEG-3 cells. Unlabeled cells with MEM-G/9 Ab incubated with IgG-MNPs (A) and JEG-3 cells incubated with the BSA-blocked MNPs without MEM-G/9 antibody conjugation (C) (as controls). Tendency of the MNPs conjugated indirectly to MEM-G/9 to target JEG-3 cells (B) and tendency of the MNPs conjugated directly to MEM-G/9 to target JEG-3 cells (D). Scale bars = 20 μm, 400× magnification.

Open Access Article. Published on 20 September 2021. Downloaded on 11/9/2025 1:16:10 AM.
This article is licensed under a Creative Commons Attribution-NonCommercial 3.0 Unported Licence.

3.5 HLA-G Ab immobilization confirmation

Although, the results of FTIR and TGA confirmed the Ab conjugation with the MNPs. We also confirmed the immobilization of the MEM-G/9 Ab onto MNPs by the immune reactivity. As depicted in Fig. 4A, Ab-MNPs showed a significant green colour. On the other hand, MNPs unconjugated with Ab (control), showed much less colour (Fig. 4B). Fluorescence intensity visualized the conjugation of MEM-G/9 on the surface of the MNPs. In addition, the findings indicated that the FITC-goat anti mouse IgG secondary Ab significantly detected the MEM-G/9 Ab immobilized on the surface of the MNPs and the conjugated Ab maintained its inherent immune reactivity to the secondary Ab.[47] Also, the negligible adsorption between FITC-IgG and the MNPs displayed the favored blocking of the MNPs with BSA. In general, the immobilization was successful.

3.6 The Ab-MNPs ability to target the HLA-G positive cells

To assess of the Ab-MNPs tendency to HLA-G positive cells, a cell binding experiment was conducted, as described in the methods section. Light microscopy images showed appropriate targeting of MEM-G/9-MNPs to JEG-3 cells (HLA-G-positive) (Fig. 5B and D). Controls also showed very little binding to target cells as expected (Fig. 5A and C). The targeting of MNPs conjugated directly to MEM-G/9 (Fig. 5D) was less than MNPs conjugated indirectly to MEM-G/9 (Fig. 5B). This lower tendency may be due to the loss of biological function of a number of directly immobilized MEM-G/9 Abs. Because Ab immobilization in this study was performed randomly through Ab amine groups, covalent binding may have occurred through some amine groups located in the Ag-binding sites.[83] As a result, it can be concluded that the activity of Fab portions of a number of MEM-G/9 antibodies was not maintained after being conjugated to MNPs.

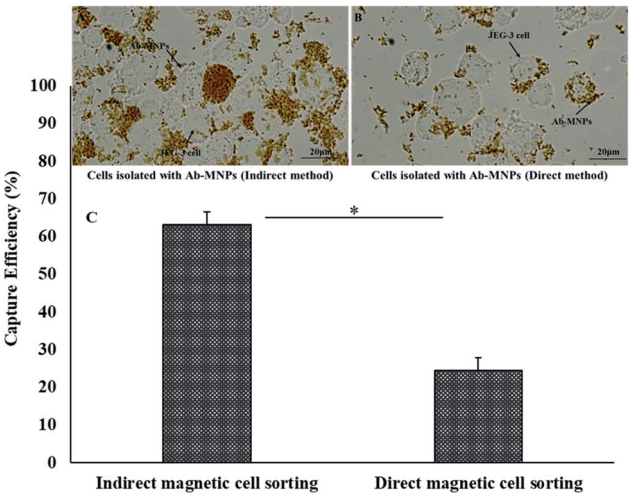

Fig. 6 Isolated JEG-3 cells by indirect immunomagnetic method (A) and by direct immunomagnetic method (B). Scale bars = 20 μm, 400× magnification. The cell capture efficiency in indirect *vs.* direct immunomagnetic method. Error bars display standard error of mean (SEM) and the asterisk displays a statistically significant difference ($p \leq 0.05$).

3.7 Cell capture efficiency of MEM-G/9-MNPs

Verification of the targeting ability of Ab-MNPs allowed the investigation of their performance in cell isolation. After incubation and magnetic separation, the capture efficiency of both direct and indirect forms of MEM-G/9-MNPs was determined with microscopy analysis (Fig. 6). The MNPs conjugated directly to MEM-G/9 captured the JEG-3 cells with an efficiency of 24.39 ± 3.41% whereas the MNPs conjugated indirectly to MEM-G/9 captured the JEG-3 cells with an efficiency of 63.07 ± 3.5%. Values are a mean efficiency of three experiments (%) ± standard error of mean (SEM). The *t*-test analysis showed that the *P*-value between the capture efficiency of direct and indirect forms of MEM-G/9-MNPs was less than 0.05 (p value = 0.01). The direct conjugation of MEM-G/9 Abs to MNPs may affect their binding affinity to HLA-G Ag and thus the capture efficiency.

3.8 Selective isolation of HLA-G$^+$ cells from HLA-G$^-$ cells with MEM-G/9-MNPs

The prepared Ab-MNPs' specificity for HLA-G$^+$ cell separation was determined by incubating a mixture of JEG-3 (HLA-G$^+$) and SKBR-3 (HLA-G$^-$) cells with the Ab-MNPs and then magnetic isolation and microscopic imaging, as mentioned in the methods section. Since the SKBR-3 cells were stained with PI and JEG-3 cells with DAPI, they

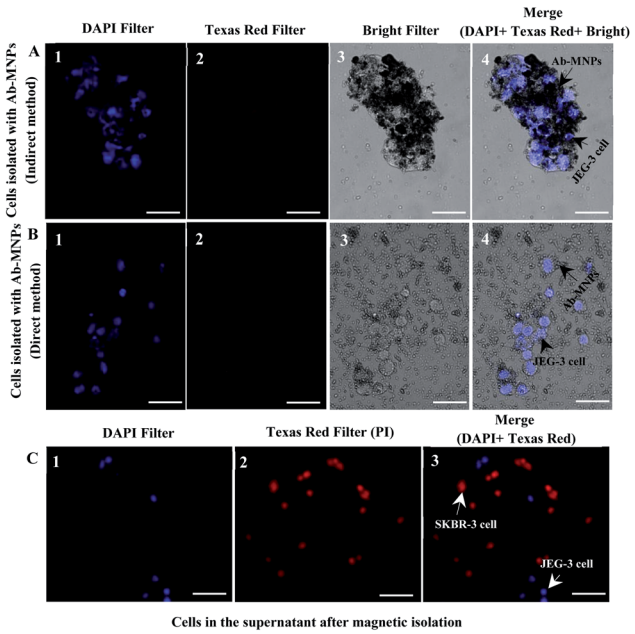

Fig. 7 The fluorescent images of cells in the precipitates after incubation with Ab-MNPs and separation under magnetic field. (A) The target JEG-3 cells isolated with the MNPs conjugated indirectly to MEM-G/9 from the non-target SKBR-3 cells (1–4). (B) The target JEG-3 cells isolated with the MNPs conjugated directly to MEM-G/9 (1–4). JEG-3 (DAPI = blue), SKBR-3 (PI = red) and MNPs (grey dots). Scale bars = 50 μm, 100× magnification. (C) The fluorescent image of cells in the supernatant after incubation with Ab-MNPs and separation under magnetic field. The HLA-G-positive JEG-3 cells not isolated by the Ab-MNPs (DAPI = blue) (1). The non-target SKBR-3 cells not isolated by the Ab-MNPs (PI = red) (2). Section (3) is a merging of (1) and (2) images. Scale bars = 50 μm, 100× magnification.

 © 2021 The Author(s). Published by the Royal Society of Chemistry

Open Access Article. Published on 20 September 2021. Downloaded on 11/9/2025 1:16:10 AM.
This article is licensed under a Creative Commons Attribution-NonCommercial 3.0 Unported Licence.

were visualized with diverse fluorescent dyes under various excitation wavelengths.[84] Fluorescence microscopy images after the magnetic isolation from the precipitates showed that blue fluorescent-stained (HLA-G$^+$) cells could be isolated by the Ab-MNPs (Fig. 7A and B), although most of the cells in the supernatant were the red fluorescent-stained (HLA-G$^-$) cells (Fig. 7C). The specificity of the prepared Ab-MNPs to isolate HLA-G$^+$ cells was verified. The MNPs conjugated indirectly to MEM-G/9 had more selective isolation than the MNPs conjugated directly to MEM-G/9. Considering that the limited number of the HLA-G$^+$ cells was not isolated by the MNPs conjugated indirectly to MEM-G/9, the MNPs conjugated indirectly to MEM-G/9 have good target specificity and are the suitable and low-cost tools for detecting and isolating target cells.

4 Conclusions

Isolation of fetal cells from maternal cells in endocervical sample remains a problem for prenatal diagnosis. MNPs have been widely used in cell isolation. Several studies have presented the successful covalent immobilization of different biologically active macromolecules (lipase,[82] albumin,[68] xylanase[36] and glucose oxidase[37]) on triazine-functionalized magnetic NPs. In the present research, similar to the studies mentioned above, triazine-functionalized magnetic NPs were used as a support for covalent immobilization of MEM-G/9 and anti-mouse IgG Abs so that the development of immunomagnetic NPs for the isolation of JEG-3 cells (trophoblastic model system) and a simple and low-cost cell isolation system based on MNPs were exhibited due to the intrinsic Ab–Ag interaction. However, several studies have been performed to isolate fetal cells with immunomagnetic nanoparticles.[20,85–92] This study was an attempt to improve isolation efficiency and cost decrease. After confirming the successful Ab-MNPs synthesis by characterization techniques and high immobilization efficiency of Abs by Bradford assay, the Ab-MNPs were used for cell isolation. The most considerable problem was the accumulation of MNP-Ab. The accumulation problem was partly removed by shaking before interaction with target cells and during incubation.

The cell capture efficiency of our synthetic MNPs in the direct immunomagnetic method was 24.39% and in the indirect method 63.07%. In the indirect immunomagnetic method, antibody targeting activity was maintained, so their capture efficiency was higher than the direct immunomagnetic method. The results were confirmed by fluorescent microscopy. The improvement in isolation and clinical applicability for prenatal diagnosis could be achieved by further optimization and the elimination of accumulation problem of prepared Ab-MNPs and assessing their reliability for the isolation of EVT cells in actual samples. The MNPs with indirect conjugate strategy also have the potential to be used for other isolation by specific Abs of the target. So, they can be considered as an efficient tool for the isolation of cells and biomolecules.

Conflicts of interest

The authors declare that they have no conflict of interest.

Author contributions

E. E: conceptualization, methodology, formal analysis, investigation, data curation, writing – original draft; A. K. B.: conceptualization, methodology, formal analysis, resources, writing – review & editing. H. N.: methodology, investigation, resources; A. Sh.: investigation; A. T. K.: investigation; S. M. K.: conceptualization, resources, project administration, writing – review & editing.

Acknowledgements

This research was supported in part by a grant for PhD candidates (project number 4504) from Shahid Sadoughi University of Medical Sciences, Yazd, Iran.

References

1 J. S. Brandt, M. A. Cruz Ithier, T. Rosen and E. Ashkinadze, *Prenatal Diagn.*, 2019, **39**, 81–87.
2 J. M. Bolnick, B. A. Kilburn, S. Bajpayee, N. Reddy, R. Jeelani, B. Crone, N. Simmerman, M. Singh, M. P. Diamond and D. R. Armant, *Fertil. Steril.*, 2014, **102**, 135–142.
3 S. Lou, C. P. Nielsen, L. Hvidman, O. B. Petersen and M. B. Risør, *BMC Pregnancy Childbirth*, 2016, **16**, 1–8.
4 K. Wou, J. L. Feinberg, R. J. Wapner and J. L. Simpson, *Expert Rev. Mol. Diagn.*, 2015, **15**, 989–998.
5 S. Drewlo and D. R. Armant, *Placenta*, 2017, **60**, S27–S31.
6 A. C. o. Obstetricians and Gynecologists, *Obstet. Gynecol.*, 2007, **110**, 1459.
7 M. Sbracia, F. Scarpellini, S. Lalwani, J. Grasso and L. Scarpellini, *Ann. N. Y. Acad. Sci.*, 1994, **731**, 170–174.
8 Y. Koumantaki, S. Sifakis, G. Dragatis, I. Matalliotakis, G. Froudarakis, E. Papadopoulou and E. Koumantakis, Prenatal Diagnosis: Published in Affiliation With the, *International Society for Prenatal Diagnosis*, 2001, **21**, 566–570.
9 C. Bussani, R. Cioni, B. Scarselli, F. Barciulli, S. Bucciantini, P. Simi, A. Fogli and G. Scarselli, Prenatal Diagnosis: Published in Affiliation With the, *International Society for Prenatal Diagnosis*, 2002, **22**, 1098–1101.
10 D. R. Armant and M. P. Diamond, *US Pat.* No. 10344315, U.S. Patent and Trademark Office, Washington, DC, 2019.
11 E. R. Norwitz and B. Levy, *Reviews in Obstetrics and Gynecology*, 2013, **6**, 48.
12 A. Obstetricians, *Obstet. Gynecol.*, 2012, **120**, 1532–1534.
13 E. Wang, A. Batey, C. Struble, T. Musci, K. Song and A. Oliphant, *Prenatal Diagn.*, 2013, **33**, 662–666.
14 M. E. Norton, N. C. Rose and P. Benn, *Obstet. Gynecol.*, 2013, **121**, 847–850.
15 A. N. Imudia, S. Kumar, M. P. Diamond, A. H. DeCherney and D. R. Armant, *Fertil. Steril.*, 2010, **93**, 1725–1730.
16 L. B. Shettles, *Nature*, 1971, **230**, 52–53.
17 A. Tarrade, R. L. Kuen, A. Malassiné, V. Tricottet, P. Blain, M. Vidaud and D. Evain-Brion, *Lab. Invest.*, 2001, **81**, 1199–1211.
18 G. Moser, S. Drewlo, B. Huppertz and D. R. Armant, *Hum. Reprod. Update*, 2018, **24**, 484–496.

Open Access Article. Published on 20 September 2021. Downloaded on 11/9/2025 1:16:10 AM.
This article is licensed under a Creative Commons Attribution-NonCommercial 3.0 Unported Licence.

19 A. N. Imudia, Y. Suzuki, B. A. Kilburn, F. D. Yelian, M. P. Diamond, R. Romero and D. R. Armant, *Hum. Reprod.*, 2009, **24**, 2086–2092.
20 P. Schueler, D. Yamanishi, J. Pearson, Y. Lee, X. Wu, S. Hashima, M. Madlansacay, C. Cain, E. Collarini and L. Foltz, *Placenta*, 2001, **22**, 702–715.
21 J. N. Bulmer, R. Cioni, C. Bussani, V. Cirigliano, F. Sole, C. Costa, P. Garcia and M. Adinolfi, *Prenatal Diagn.*, 2003, **23**, 34–39.
22 M. G. Katz-Jaffe, D. Mantzaris and D. S. Cram, *BJOG*, 2005, **112**, 595–600.
23 A. Grützkau and A. Radbruch, *Cytometry, Part A*, 2010, **77**, 643–647.
24 B. D. Plouffe, S. K. Murthy and L. H. Lewis, *Rep. Prog. Phys.*, 2014, **78**, 016601.
25 R. David, M. Groebner and W. M. Franz, *Stem Cells*, 2005, **23**, 477–482.
26 S. Miltenyi, W. Müller, W. Weichel and A. Radbruch, *Cytometry*, 1990, **11**, 231–238.
27 H. Shahrestani, A. Taheri-Kafrani, A. Soozanipour and O. Tavakoli, *Biochem. Eng. J.*, 2016, **109**, 51–58.
28 H. Guo, Y. Tang, Y. Yu, L. Xue and J.-q. Qian, *Int. J. Biol. Macromol.*, 2016, **87**, 537–544.
29 U. Jinendra, J. Kumar, B. Nagabhushana, A. V. Raghu and D. Bilehal, *Green Mater.*, 2019, **7**, 137–142.
30 K. Kannan, D. Radhika, K. R. Reddy, A. V. Raghu, K. K. Sadasivuni, G. Palani and K. Gurushankar, *Nano Express*, 2021, **2**, 010014.
31 C. T. Yavuz, J. Mayo, W. Y. William, A. Prakash, J. C. Falkner, S. Yean, L. Cong, H. J. Shipley, A. Kan and M. Tomson, *Science*, 2006, **314**, 964–967.
32 S. Trabulo, A. Aires, A. Aicher, C. Heeschen and A. L. Cortajarena, *Biochim. Biophys. Acta*, 2017, **1861**, 1597–1605.
33 U. Jinendra, D. Bilehal, B. Nagabhushana, K. R. Reddy, C. V. Reddy and A. V. Raghu, *Mater. Sci. Energy Technol.*, 2019, **2**, 657–666.
34 L. S. Ganapathe, M. A. Mohamed, R. Mohamad Yunus and D. D. Berhanuddin, *Magnetochemistry*, 2020, **6**, 68.
35 M. Mostafaei, S. N. Hosseini, M. Khatami, A. Javidanbardan, A. A. Sepahy and E. Asadi, *Protein Expression Purif.*, 2018, **145**, 1–6.
36 A. Soozanipour, A. Taheri-Kafrani and A. L. Isfahani, *Chem. Eng. J.*, 2015, **270**, 235–243.
37 M. Abbasi, R. Amiri, A.-K. Bordbar, E. Ranjbakhsh and A.-R. Khosropour, *Appl. Surf. Sci.*, 2016, **364**, 752–757.
38 F. Shamsipour, A. H. Zarnani, R. Ghods, M. Chamankhah, F. Forouzesh, S. Vafaei, A. A. Bayat, M. M. Akhondi, M. A. Oghabian and M. Jeddi-Tehrani, *Avicenna J. Med. Biotechnol.*, 2009, **1**, 27.
39 X. Hou, C. Zhao, Y. Tian, S. Dou, X. Zhang and J. Zhao, *Chem. Res. Chin. Univ.*, 2016, **32**, 889–894.
40 Y. Wang and B. Liu, *Biosens. Bioelectron.*, 2009, **24**, 3293–3298.
41 S. Taebi, M. Keyhanfar and A. Noorbakhsh, *J. Immunol. Methods*, 2018, **458**, 26–32.
42 Y. Loke, A. King, T. Burrows, L. Gardner, M. Bowen, S. Hiby, S. Howlett, N. Holmes and D. Jacobs, *Tissue Antigens*, 1997, **50**, 135–146.
43 S. Hiby, A. King, A. Sharkey and Y. Loke, *Tissue Antigens*, 1999, **53**, 1–13.
44 I. K. Marcinkowskiego, *Isolation of Fetus Cells from Maternal Blood Pre-clinical Study*, PhD thesis in Nanobiotechnology, Poznan University of Medical Sciences, 2011.
45 S. R. Makhsin, P. L. Teoh and K. A. Razak, *Reviews in Advanced Sciences and Engineering*, 2015, **4**, 3–21.
46 M. H. Jazayeri, H. Amani, A. A. Pourfatollah, H. Pazoki-Toroudi and B. Sedighimoghaddam, *Sensing and Bio-Sensing Research*, 2016, **9**, 17–22.
47 M. Poplawska, M. Bystrzejewski, I. P. Grudziński, M. A. Cywińska, J. Ostapko and A. Cieszanowski, *Carbon*, 2014, **74**, 180–194.
48 H. Xu, Z. P. Aguilar, L. Yang, M. Kuang, H. Duan, Y. Xiong, H. Wei and A. Wang, *Biomaterials*, 2011, **32**, 9758–9765.
49 A. Schaetz, M. Hager and O. Reiser, *Adv. Funct. Mater.*, 2009, **19**, 2109–2115.
50 D. Predoi, *Dig. J. Nanomater. Biostructures*, 2007, **2**, 169–173.
51 M. Jonnalagadda, V. B. Prasad and A. V. Raghu, *J. Mol. Struct.*, 2021, **1230**, 129875.
52 K. Kannan, D. Radhika, A. Nesaraj, K. K. Sadasivuni, K. R. Reddy, D. Kasai and A. V. Raghu, *Mater. Sci. Energy Technol.*, 2020, **3**, 853–861.
53 Y. Chi, Q. Yuan, Y. Li, J. Tu, L. Zhao, N. Li and X. Li, *J. Colloid Interface Sci.*, 2012, **383**, 96–102.
54 S. Hou, X. Li, H. Wang, M. Wang, Y. Zhang, Y. Chi and Z. Zhao, *RSC Adv.*, 2017, **7**, 51993–52000.
55 F. J. Sharahi and A. Shahbazi, *Chemosphere*, 2017, **189**, 291–300.
56 D. Burt, D. Johnston, T. R. de Wit, P. van den Elsen and P. L. Stern, *Int. J. Cancer*, 1991, **47**, 117–122.
57 C. Menier, B. Saez, V. Horejsi, S. Martinozzi, I. Krawice-Radanne, S. Bruel, C. Le Danff, M. Reboul, I. Hilgert and M. Rabreau, *Hum. Immunol.*, 2003, **64**, 315–326.
58 R. Apps, S. P. Murphy, R. Fernando, L. Gardner, T. Ahad and A. Moffett, *Immunology*, 2009, **127**, 26–39.
59 N. Nazari and S. Farjadian, *Iran. J. Immunol.*, 2016, **13**, 178–185.
60 S. Ghoshdastidar, *Clinical translation of nanomaterials for early detection of genetic abnormalities in fetus and retinopathy in neonates and adults*, PhD thesis, University of Missouri-Columbia, 2017.
61 L. Thiruchelvam-Kyle, S. E. Hoelsbrekken, P. C. Saether, E. G. Bjørnsen, D. Pende, S. Fossum, M. R. Daws and E. Dissen, *J. Immunol.*, 2017, **198**, 2556–2567.
62 J. Xu, C. Ju, J. Sheng, F. Wang, Q. Zhang, G. Sun and M. Sun, *Bull. Korean Chem. Soc.*, 2013, **34**, 2408–2412.
63 M. Yamaura, R. Camilo, L. Sampaio, M. Macedo, M. Nakamura and H. Toma, *J. Magn. Magn. Mater.*, 2004, **279**, 210–217.
64 J. Zhao, Y. Gui, Y. Liu, G. Wang, H. Zhang, Y. a. Sun and S. Fang, *Catal. Lett.*, 2017, **147**, 1127–1132.
65 A. H. Gemeay, B. E. Keshta, R. G. El-Sharkawy and A. B. Zaki, *Environ. Sci. Pollut. Res.*, 2019, 1–18.

 © 2021 The Author(s). Published by the Royal Society of Chemistry

Open Access Article. Published on 20 September 2021. Downloaded on 11/9/2025 1:16:10 AM.
This article is licensed under a Creative Commons Attribution-NonCommercial 3.0 Unported Licence.

66 A. Raghu, G. Gadaginamath, N. Mallikarjuna and T. Aminabhavi, *J. Appl. Polym. Sci.*, 2006, **100**, 576–583.
67 A. Raghu and H. M. Jeong, *J. Appl. Polym. Sci.*, 2008, **107**, 3401–3407.
68 A. Bordbar, A. Rastegari, R. Amiri, E. Ranjbakhsh, M. Abbasi and A. Khosropour, *Biotechnol. Res. Int.*, 2014, 2014.
69 M. Amirbandeh and A. Taheri-Kafrani, *Int. J. Biol. Macromol.*, 2016, **93**, 1183–1191.
70 K. Mu, S. Zhang, T. Ai, J. Jiang, Y. Yao, L. Jiang, Q. Zhou, H. Xiang, Y. Zhu and X. Yang, *Mol. Imaging*, 2015, **14**, 7290.
71 N. A. Frey, S. Peng, K. Cheng and S. Sun, *Chem. Soc. Rev.*, 2009, **38**, 2532–2542.
72 W. Liu, L. Nie, F. Li, Z. P. Aguilar, H. Xu, Y. Xiong, F. Fu and H. Xu, *Biomater. Sci.*, 2016, **4**, 159–166.
73 Y. Teng, C. Jiang, A. Ruotolo and P. W. Pong, *IEEE Trans. Nanotechnol.*, 2016, **17**, 69–77.
74 Y. Kobayashi, H. Inose, T. Nakagawa, K. Gonda, M. Takeda, N. Ohuchi and A. Kasuya, *J. Colloid Interface Sci.*, 2011, **358**, 329–333.
75 M. Susewind, A.-M. Schilmann, J. Heim, A. Henkel, T. Link, K. Fischer, D. Strand, U. Kolb, M. N. Tahir and J. Brieger, *J. Mater. Chem. B*, 2015, **3**, 1813–1822.
76 J. H. Min, M.-K. Woo, H. Y. Yoon, J. W. Jang, J. H. Wu, C.-S. Lim and Y. K. Kim, *Anal. Biochem.*, 2014, **447**, 114–118.
77 W. Sheng, W. Wei, J. Li, X. Qi, G. Zuo, Q. Chen, X. Pan and W. Dong, *Appl. Surf. Sci.*, 2016, **387**, 1116–1124.
78 C. Meng, W. Zhikun, L. Qiang, L. Chunling, S. Shuangqing and H. Songqing, *J. Hazard. Mater.*, 2018, **341**, 198–206.
79 F. Golmohammadi, M. Hazrati and M. Safari, *Microchem. J.*, 2019, **144**, 64–72.
80 S. A. A. Noma, A. Ulu, S. Koytepe and B. Ateş, *Biocatal. Biotransform.*, 2020, **38**, 392–404.
81 M. A. Ghasemzadeh, M. H. Abdollahi-Basir and M. Babaei, *Green Chem. Lett. Rev.*, 2015, **8**, 40–49.
82 E. Ranjbakhsh, A. Bordbar, M. Abbasi, A. Khosropour and E. Shams, *Chem. Eng. J.*, 2012, **179**, 272–276.
83 S. Jeong, J. Y. Park, M. G. Cha, H. Chang, Y.-i. Kim, H.-M. Kim, B.-H. Jun, D. S. Lee, Y.-S. Lee and J. M. Jeong, *Nanoscale*, 2017, **9**, 2548–2555.
84 B. S. Cummings and R. G. Schnellmann, *Curr. Protoc. Pharmacol.*, 2004, **25**, 12–18.
85 R. Kannan, S. Ghoshdastidar, D. Suresh, D. Schust and A. Upendran, *US Pat.*, **15/150262**.
86 U. Mueller, C. Hawes, A. Wright, E. DeBoni, W. Jones, F. Firgaira, A. Morley and D. Turner, *Lancet*, 1990, **336**, 197–200.
87 D. Gänshirt-Ahlert, M. Burschyk, H. S. Garritsen, L. Helmer, P. Miny, J. Horst, H. P. Schneider and W. Holzgreve, *Am. J. Obstet. Gynecol.*, 1992, **166**, 1350–1355.
88 Y. Zheng, N. P. Carter, C. M. Price, S. M. Colman, P. J. Milton, G. A. Hackett, M. F. Greaves and M. A. Ferguson-Smith, *J. Med. Genet.*, 1993, **30**, 1051–1056.
89 J. Büsch, P. Huber, E. Pflüger, S. Miltenyi, J. Holtz and A. Radbruch, *Prenatal Diagn.*, 1994, **14**, 1129–1140.
90 C. S. Hawes, H. Suskin, B. Kalionis, U. Mueller, G. Casey, J. Hall and Z. Rudzki, *Ann. N. Y. Acad. Sci.*, 1994, **731**, 181–185.
91 L. Durrant, K. McDowall, R. Holmes and D. Liu, *BJOG*, 1996, **103**, 219–222.
92 T. H. Lim, A. Tan and V. H. H. Goh, *Hum. Genet.*, 1999, **104**, 399–404.